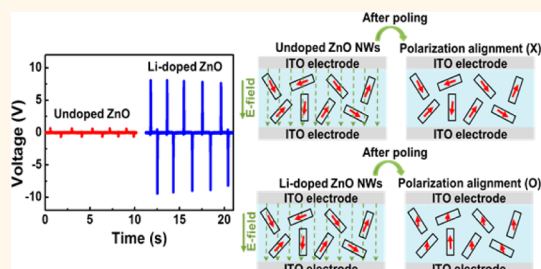


Lithium-Doped Zinc Oxide Nanowires–Polymer Composite for High Performance Flexible Piezoelectric Nanogenerator

Sung-Ho Shin,[†] Young-Hwan Kim,[†] Min Hyung Lee,[‡] Joo-Yun Jung,[§] Jae Hun Seol,^{||} and Junghyo Nah^{*,†}

[†]Department of Electrical Engineering, Chungnam National University, Yuseong-Gu, Daejeon 305-764, Korea, [‡]Department of Applied Chemistry, Kyung Hee University, Yongin, Gyeonggi 446-701, Korea, [§]Department of Nano Manufacturing Technology, Korea Institute of Machinery and Materials, Yuseong-Gu, Daejeon 305-343, Korea, and ^{||}School of Mechatronics, Gwangju Institute of Science and Technology (GIST), Buk-gu, Gwangju 500-712, Korea

ABSTRACT We present a method to develop high performance flexible piezoelectric nanogenerators (NGs) by employing Li-doped ZnO nanowires (NWs). We synthesized Li-doped ZnO NWs and adopted them to replace *intrinsic* ZnO NWs with a relatively low piezoelectric coefficient. When we exploited the ferroelectric phase transition induced in Li-doped ZnO NWs, the performance of the NGs was significantly improved and the NG fabrication process was greatly simplified. In addition, our approach can be easily expanded for large-scale NG fabrication. Consequently, the NGs fabricated by our simple method exhibit the excelling output voltage and current, which are stable and reproducible during periodic bending/releasing measurement over extended cycles. In addition, output voltage and current up to ~ 180 V and ~ 50 μ A, respectively, were obtained in the large-scale NG. The approach introduced here extends the performance limits of ZnO-based NGs and their potentials in practical applications.



KEYWORDS: piezoelectric nanogenerator · lithium doped zinc oxide nanowires · ferroelectricity · flexible electronics

Zinc oxide (ZnO) has been demonstrated as one of the most promising materials for the realization of piezoelectric energy harvesting devices, due to its environmentally safe nature, abundance, mechanical robustness, and low permittivity.^{1–6} Thus, piezoelectric nanogenerators (NGs) based on ZnO have been actively investigated to date.^{7–12} However, the piezoelectric potential screening in *intrinsic* ZnO¹³ inhibited the realization of high performance piezoelectric NGs. Therefore, consistent efforts have been made to overcome this fundamental limitation and thereby enhance the output performance of ZnO-based piezoelectric NGs. For instance, several approaches, such as surface O₂ plasma treatment,¹⁴ p–n junction formation,^{15,16} and triboelectric layer insertion,¹⁷ have been adopted to boost piezoelectric output power. However, performance enhancement of ZnO-based piezoelectric NGs has still been hindered due to its inherently low piezoelectric coefficient¹⁸ by

comparison to other well-known piezoelectric materials such as PbZr_xTi_{1-x}O₃ (PZT)¹⁹ and BaTiO₃.²⁰

Previously, it was reported that ZnO with the wurtzite crystal structure, which inherently reveals piezoelectric property along the *c*-axis,²¹ can be doped with lithium (Li) and the ferroelectric phase transition can be induced in Li-doped ZnO. This phase transition is originated by atomic replacement in ZnO by substitution of the Zn atoms with introduced off-centered Li atoms, enabled by the large difference in ionic radii between Zn (0.74 Å) and Li (0.60 Å).^{22,23} By exploiting this finding, we first employ the Li-doped ZnO nanowires (NWs) for piezoelectric NG fabrication to extend performance limits of the ZnO-based NGs. Here, with the use of the composite solution prepared by mixing hydrothermally grown Li-doped ZnO NWs and polydimethylsiloxane (PDMS) polymer, the NGs were fabricated by simply spin-coating the solution on the electrode layers, followed by curing

* Address correspondence to jnah@cnu.ac.kr.

Received for review August 19, 2014 and accepted September 29, 2014.

Published online September 29, 2014
10.1021/nn5046568

© 2014 American Chemical Society

and high voltage poling steps. Owing to ferroelectricity in Li-doped ZnO NWs, it can be poled under high electric field to maximize piezoelectric behavior. The spontaneous polarization induced in Li-doped ZnO NWs improves piezoelectric coefficient (d_{33}),²⁴ which plays an important role in performance enhancement of the NGs. In addition, it can greatly relieve the requirement for *c*-axis orientation of undoped ZnO NWs onto substrates in order to maximize output power generation. Therefore, our simple approach provides two distinct advantages over previously reported undoped ZnO-based flexible piezoelectric NGs. First, the performance of the NGs is significantly enhanced by spontaneous polarization in Li-doped ZnO NWs. Second, the NG fabrication process is greatly simplified and can be easily expanded in large-scale.

Our NGs demonstrate open-circuit voltage (V_{oc}) of ~ 180 V and short-circuit current (I_{sc}) of ~ 50 μ A during the periodic bending condition (active area of $10\text{ cm} \times 10\text{ cm}$). Stable and reproducible output voltage and current were also confirmed during the cyclic measurement over 1350 cycles per each run, which was repeated over 4 weeks. The approach introduced here extends performance limits of ZnO-based piezoelectric NGs, which also provides a simple, cost-effective, and suitable way to fabricate large-scale flexible NGs.

RESULT AND DISCUSSION

The NG fabrication is schematically shown in Figure 1a. First, Li-doped ZnO NWs were synthesized by solution-based hydrothermal method, followed by high temperature annealing step at $550\text{ }^{\circ}\text{C}$ for 1 h 30 min in O_2 ambient. The annealing step promotes activation of lithium atoms in the wurtzite crystal structure.²⁵ The detailed Li-doped ZnO NW growth

recipe is described in the experimental method. Different from typical NW growth on the substrate coated with a seed layer,^{26,27} the NWs here were grown in the solution with zinc nitrate as seed reagent. Next, after drying and cleaning steps, the synthesized Li-doped ZnO NWs were mixed well with PDMS. The composite solution was then spin-coated on the indium tin oxide (ITO)-coated PET substrate, which was pre-cleaned by acetone, IPA, and deionized (DI) water, respectively. Lastly, an ITO coated PET substrate was pasted on the opposite side of the device as a counter electrode, followed by curing in a convection oven, which finalizes the NG fabrication. The detailed device fabrication process is described in the experimental method. The as-fabricated device is flexible and semitransparent (Figure 1b). The scanning electron micrograph (SEM) in Figure 1c shows the synthesized Li-doped ZnO NWs, revealing hexagonal wurtzite crystal structure [Figure 1c (inset)]. The building blocks of the fabricated piezoelectric NG consist of two main parts (Figure 1d): two ITO (100 nm)-coated PET substrates with a thickness of $\sim 170\text{ }\mu\text{m}$ and the composite layer made of Li-doped ZnO NWs and PDMS. The dispersed Li-doped ZnO NWs inside PDMS can be observed in a cross-sectional SEM (Supporting Information Figure S1).

To determine proper Li-doping condition, Li-doped ZnO NWs were synthesized by varying the concentration of lithium nitrate (LiNO_3) from 0 to 75 mM while maintaining the same zinc nitrate ($\text{Zn}(\text{NO}_3)_2$) concentration (50 mM). We note that other experimental conditions were kept the same during the growth process. With the use of room temperature photoluminescence (PL) spectroscopic analysis, the doping related optical properties of the NWs were characterized (Figure 2a–c). The strong ultraviolet (UV)

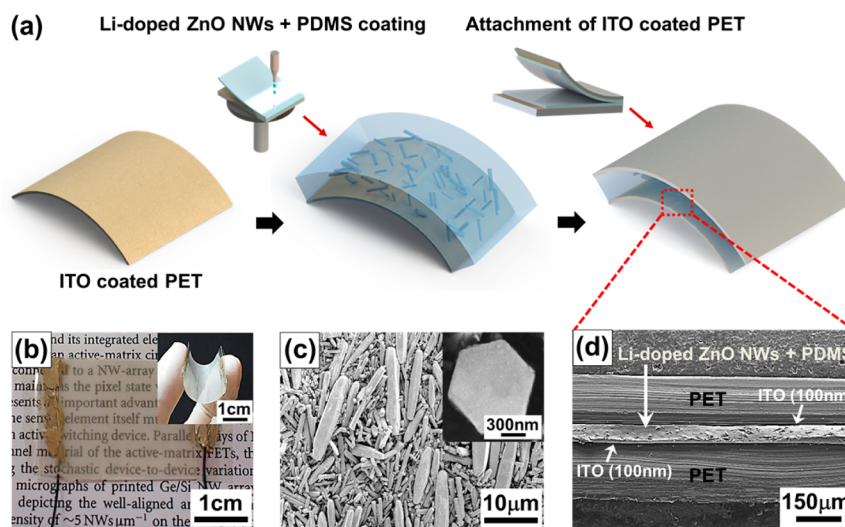


Figure 1. (a) Schematic representation of the NG fabrication process: composite layer, containing Li-doped ZnO NWs and PDMS, is sandwiched between two electrode layers. (b) Photograph of the fabricated NG exhibiting semitransparency and flexibility (inset). (c) SEM of hydrothermally synthesized Li-doped ZnO NWs after cleaning and drying steps. The inset shows hexagonal-shaped Li-doped ZnO with the wurtzite crystal structure. (d) A cross-sectional SEM of the fabricated NG where the composite layer is sandwiched between ITO-coated PET films as top and bottom electrodes.

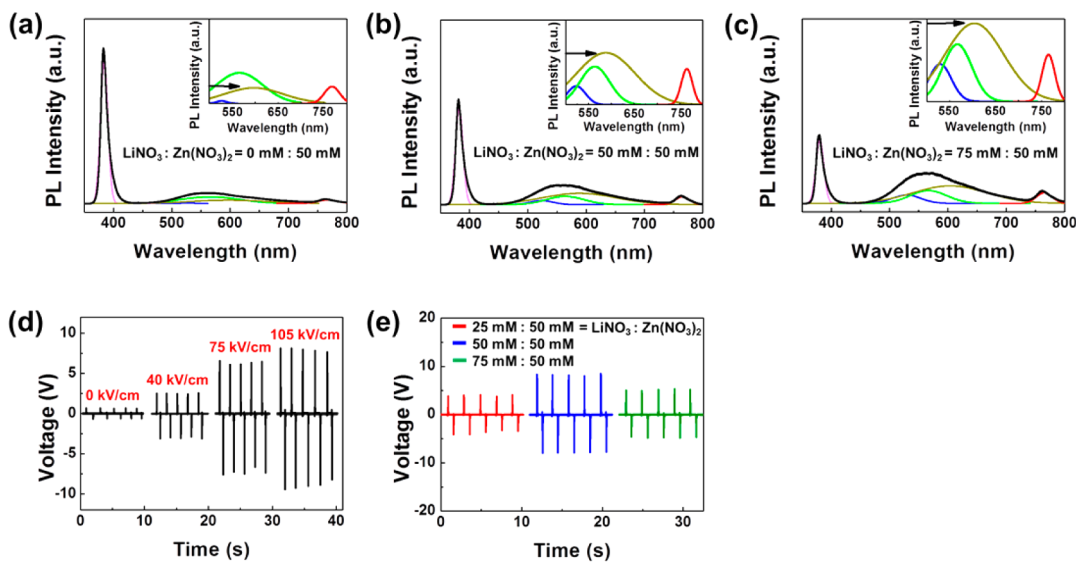


Figure 2. (a) PL spectra for ZnO NWs synthesized by varying the concentration ratio between LiNO_3 and $\text{Zn}(\text{NO}_3)_2$ as (a) 0:50 mM, (b) 50:50 mM, and (c) 75:50 mM. The Gaussian fitting curves are used to clarify the emission lines. The insets show magnified Gaussian fitting curves for the wavelength range between 500 and 800 nm. The yellow intensity (marked with the arrows) gradually increases as the LiNO_3 concentration is increased, indicating lithium incorporation in ZnO NWs. (d) The output voltage increases in proportion to the applied electric field, demonstrating poling effect and ZnO NW doping with Li. The NG was fabricated using the NWs synthesized in the solution with $\text{LiNO}_3:\text{Zn}(\text{NO}_3)_2 = 50:50$ mM. (e) Output voltage dependence on Li concentration in the NW synthesis solution. Each NG was fabricated using the NWs synthesized at different concentration of LiNO_3 : 25, 50, and 75 mM, respectively.

emissions were observed near ~ 380 nm, which are related to near band edge excitonic emissions.²⁸ As the lithium concentration increases, the UV emission peaks in Li-doped ZnO NWs were shifted to higher photon energy from 3.18 eV (Figure 2a) to 3.25 eV (Figure 2c), indicating a broadening of the optical band gap.²⁸ The PL spectra in broadband emission (500–800 nm) are related to the defects in the ZnO crystal. Specifically, the blue emission (420–500 nm)²⁹ and green emission (480–600 nm)³⁰ have been reported to originate from interstitial Zn ions of ZnO crystals and oxygen vacancy (V_O), respectively. The red emission is attributed to excess oxygen on the ZnO surface.³¹ The yellow emission in Figure 2a for undoped ZnO NWs (yellow solid line) can be due to the OH group.³² On the other hand, the relatively high intensity of yellow emissions in Figure 2(b,c) is due to both substitutional Li (Li_{Zn}) and interstitial Li (Li_i) in the ZnO crystal since the transitions from donor levels (V_o or Li_i) to Li_{Zn} acceptor levels release yellow emissions.³³ It can be obviously observed that relative intensity of yellow emission gradually increases as Li doping concentration increases. The results presented here are consistent with the study reported previously.^{28–33} Next, the NGs were fabricated using grown Li-doped ZnO NWs with different Li concentrations and were subsequently poled under high electric field to align piezoelectric domain of the NWs. Figure 2d shows the representative piezoelectric output voltages of the NGs, measured after poling under different electric fields from 0 to 105 kV cm^{-1} at 65 °C for 20 h: the NWs used here were synthesized in the solution with a

ratio of $\text{LiNO}_3:\text{Zn}(\text{NO}_3)_2 = 50:50$ mM. It can be noted that the output voltage of the NGs increases in proportion to applied poling E-field, which can also indicate that the NWs are indeed doped with Li and ferroelectric phase transition is achieved. The details of power generation mechanism of the NGs, which generate alternating current and voltage, are described in Supporting Information Figure S2. Figure 2e shows the output voltage dependence of the NGs on Li concentration in the NW synthesis solution: LiNO_3 concentration was increased from 25 to 75 mM while maintaining the same $\text{Zn}(\text{NO}_3)_2$ concentration, 50 mM. Here, all the devices, having the same dimension (2 cm \times 2 cm), were poled at 105 kV cm^{-1} and measured during periodic bending and releasing motions, induced by horizontal travel (5 mm) of the bending stage. The results show that the output voltages (V_{oc}) were clearly affected by the Li concentration in the synthesis solution (Figure 2e). The highest output voltage (~ 9 V) was observed in the NG fabricated with the NWs synthesized from the solution with $\text{LiNO}_3:\text{Zn}(\text{NO}_3)_2 = 50:50$ mM [Supporting Information Video File 1]. In case that the relative LiNO_3 concentration is 25 mM, the output voltages were reduced to ~ 4 V. The ferroelectric property is still induced here, however, it is insufficient to maximize piezoelectric output. On the other hand, at the LiNO_3 concentration of 75 mM, excessive holes and defects may be induced in the NWs, reducing the output voltage (~ 5 V) as they screen the piezoelectric output potential.³⁴ We note here that the results were confirmed in multiple devices. Besides, to ensure the validity of the generated

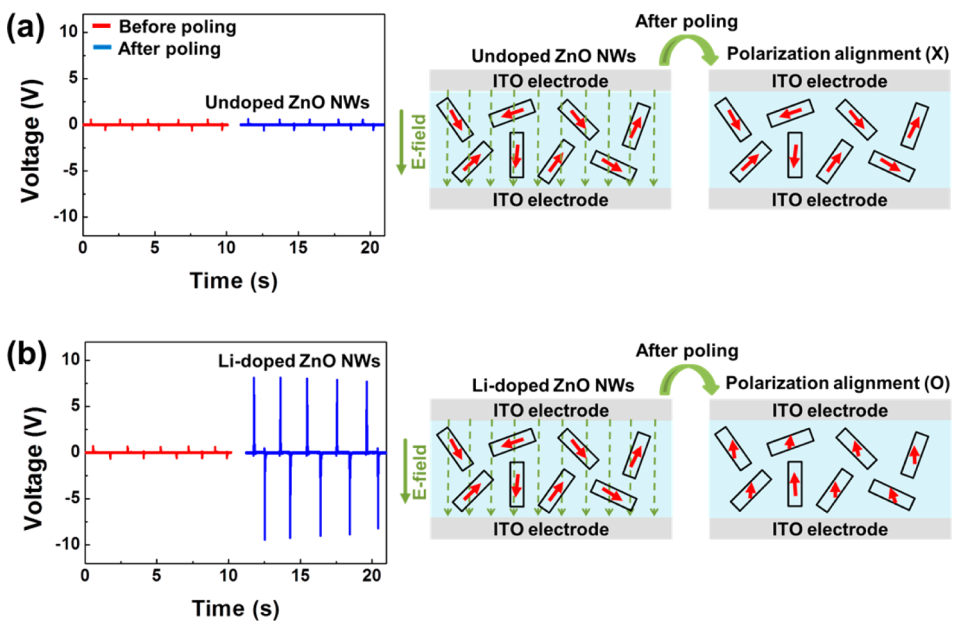


Figure 3. (a) Output voltages (on the left) of the NG fabricated with undoped ZnO NWs, not retaining ferroelectric property. Even after poling process, no difference can be observed in the generated output voltages. The schematic diagram (on the right) shows the polarization of the NWs inside the NG before/after poling process: (before) randomly oriented polarization inside PDMS (after) randomized polarization maintains inside PDMS. (b) Output voltages (on the left) of the NGs fabricated with Li-doped ZnO NWs. After poling process, the output voltage is significantly enhanced. The schematic diagram (on the right) shows the polarization of the NWs inside the NG before/after poling process: (before) randomly oriented polarization inside PDMS (after) polarization alignment inside PDMS, owing to the incorporation of lithium rendering ferroelectric property.

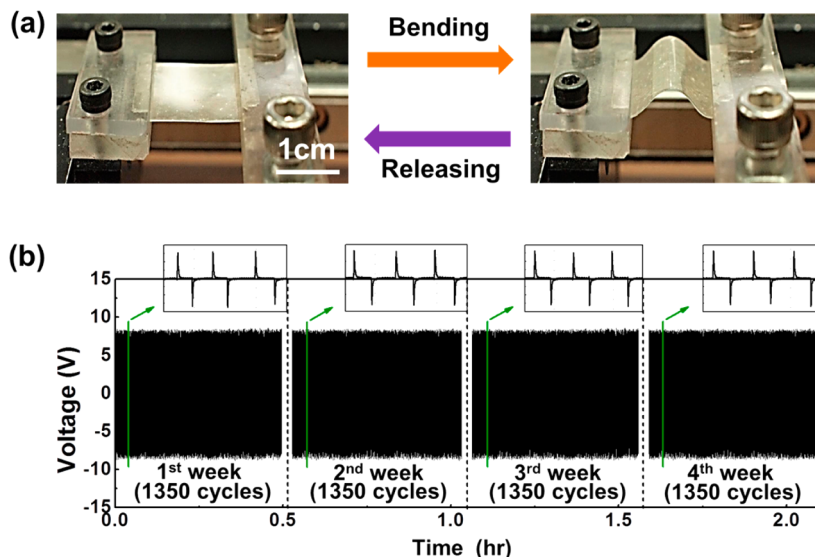


Figure 4. (a) Photographs of the NG at bending (right) and releasing states (left) mounted on the bending stage. (b) Reproducible and stable output voltage measured over 4 weeks: identical output values were measured without any performance degradation for each run (1350 cyclic measurement), repeated over 4 weeks. The insets show magnified signals of the green colored regions.

piezoelectric signals, the switching polarity test^{35,36} was performed under the reverse connection mode. The magnitude of the generated outputs was equal to that under the forward connection mode with an opposite polarity (Supporting Information Figure S3).

Figure 3 explicitly shows Li-doping effect and related piezoelectric output voltage enhancement by comparing with the *intrinsic* ZnO NW-based NG. In the case of undoped ZnO NWs not retaining ferroelectricity,

randomly oriented electric dipole state was maintained even after the poling process as a schematic drawing in Figure 3a. Thus, in undoped ZnO NWs, the poling process has no impact on piezoelectric output voltage as expected. On the contrary, the NG with Li-doped ZnO NWs after poling process generates significantly enhanced output voltage (Figure 3b). Due to the spontaneous polarization in Li-doped ZnO NWs, the randomly oriented electric dipole state can

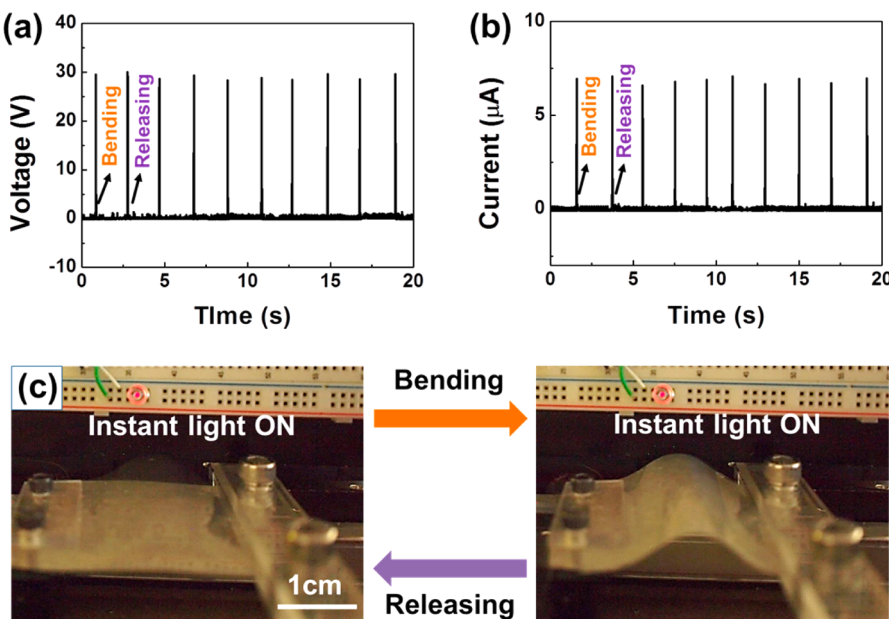


Figure 5. Output performance of the NGs with a size of $3.5\text{ cm} \times 3.5\text{ cm}$. (a) Output voltage and (b) output current during the cyclic bending and releasing motions. (c) A red LED lights up by the NG. The output of the NG was fed through a full-wave bridge rectifier circuit whose output was again connected to inputs of the LED. The LED turns on at both bending and releasing states.

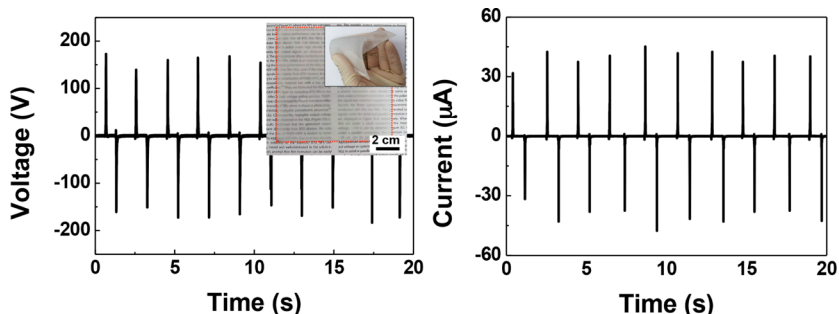


Figure 6. Output voltage (left) and current (right) of a large-scale NG. Output voltage and current up to $\sim 180\text{ V}$ and $\sim 50\text{ }\mu\text{A}$ were obtained during 30 mm horizontal travel of the bending stage. (Inset) Fabricated large-scale NG with an area of $10\text{ cm} \times 10\text{ cm}$.

be readily aligned by the externally applied high electric field between two electrodes. The results here clearly indicate the output performance enhancement of piezoelectric NG by Li-doped ZnO NWs.

In Figure 4, reliability of the NG was examined by cyclic measurement. During periodic bending and releasing motions by horizontal travel (5 mm) of moving stage (Figure 4a), the NG's output voltage was measured. For each run, the NG was measured for 1350 cycles, which were then repeated over 4 weeks to monitor any performance degradation (Figure 4b). We observed a consistent output voltage ($16\text{ V}_{\text{peak-to-peak}}$) under 0.32% strain for the entire measurement cycles, revealing superior mechanical durability of the NG. We investigated multiple devices and confirmed the stable and reproducible output signals (Supporting Information Figure S4). This is partly originated from structural advantage of the NWs and polymer composite, where PDMS prevents the NWs from cracking upon cyclic

or excessive mechanical deformation while effectively transmitting the applied force to the NWs. In addition, natural degradation of the NWs can be prohibited by PDMS encapsulation.

To boost the output power of the NG such that it can light up commercial light-emitting diode (LED) without charging capacitors, its size was enlarged to an active area of $3.5\text{ cm} \times 3.5\text{ cm}$ by simply spin-coating on a bigger substrate. We kept all other experimental conditions the same for consistency. Two output nodes of the NG were first connected to a full-wave bridge rectifier circuit, which converts AC to DC output, and the rectified output power was fed directly to a red commercial light-emitting diode (LED) (Supporting Information Figure S5). After the NG was mounted on the bending stage, the output voltage and current were measured during the periodic bending/releasing motions induced by 5 mm horizontal travel of the stage, triggering 0.19% strain. We note that increasing

the travel range of the stage accordingly increases output voltage and current (Supporting Information Figures S6 and S7). The rectified output voltage and current from the NG were, respectively, ~ 30 V and ~ 7 μ A (Figure 5a,b), which was enough to directly turn on a commercial LED without an aid of capacitor (Figure 5c and Supporting Information Video File 2). For large-scale NG demonstration, we fabricated the NG with a size of 10 cm \times 10 cm [Figure 6 (inset)]. The output voltage and current up to ~ 180 V and ~ 50 μ A were obtained during 30 mm horizontal travel of the bending stage. We expect that the NG's output power can be further increased either by enlarging active area or stacking vertically.

CONCLUSION

In summary, we have developed a novel approach to realize high performance flexible piezoelectric NGs by

employing Li-doped ZnO NWs. The output performance of the NGs was greatly improved by enhanced piezoelectric coefficient thanks to spontaneous polarization in poled Li-doped ZnO NWs. In addition, the *c*-axis orientation of ZnO NWs, required in typical ZnO NW-based NGs for maximizing output power generation, became less critical in the device design. Thus, it leads to the simplified NG fabrication process, which can be easily adopted for a large-scale device fabrication. The NWs–polymer composite structure also provides excellent durability and stability in our NGs. Further, by enlarging the size of the NG, we achieved output voltage and current up to ~ 180 V and ~ 50 μ A, respectively. Our approach provides a simple and cost-effective way to extend performance limits of ZnO-based piezoelectric NGs, which is also suitable for a large-scale NG fabrication.

EXPERIMENTAL METHODS

Li-Doped ZnO NW Synthesis. The 50 mM of zinc nitrate ($\text{Zn}(\text{NO}_3)_2 \cdot \text{H}_2\text{O}$, Sigma-Aldrich) and 50 mM of hexamethylene-tetramine (HMTA, Sigma-Aldrich) were poured into a container filled with deionized (DI) water of 50 mL. The lithium doping reagent, lithium nitrate (LiNO_3 , Sigma-Aldrich), was added to the solution. The solutions with different mixture ratios ($\text{LiNO}_3:\text{Zn}(\text{NO}_3)_2 \cdot \text{H}_2\text{O}$) were prepared: (0:50 mM), (25:50 mM), (50:50 mM), and (75:50 mM). Each solution was stirred on a hot plate at 60 °C for 2 h. Next, for the hydrothermal growth of undoped and Li-doped ZnO NWs, the solutions were kept in oven at constant temperature of 95 °C for 10 h. After the growth process, liquid content was completely removed and remaining the NW powder was subsequently cleaned with DI water and ethanol. The container was then dried in oven at 200 °C for 3 h, and then the container was cooled down to room temperature. Lastly, the grown NWs were annealed in a furnace at 550 °C for 1.5 h in oxygen atmosphere.

NG Fabrication. The NG fabrication process can be summarized as the following. First, the ITO (100 nm) coated PET substrates (Sigma-Aldrich) were cleaned by acetone, IPA, and DI water. Next, the Li-doped ZnO NWs (10 wt %) were well mixed with PDMS (Sylgard, 184 Silicon elastomer) that was prepared with a (10:1) elastomer to curing agent mixing ratio. The prepared composite solution was spin-coated on a substrate at 2500 rpm for 30 s and precured in oven at 85 °C for 5 min. The composite solution was spin-coated on another ITO (100 nm) coated PET film at 5500 rpm for 40 s, which was subsequently attached on the preformed composite thin film. Lastly, the devices were cured in oven at 85 °C for 2 h.

Characterization. The output voltage and current were measured by using a voltage meter (Agilent, 34401A) and current preamplifier (Stanford Research Systems, SR 570), respectively. The cyclic bending and releasing motions were provided by a custom-built bending stage setup. A PL spectrometer (Horiba Jobin Yvon, Inc., LabRAM HR-800) was used to analyze the PL spectra of undoped and Li-doped ZnO NWs. The PL measurement was carried out by using He–Cd laser (325 nm). The FE-SEM (Hitachi, S-4800) was used to observe Li-doped ZnO NWs and device structures.

Conflict of Interest: The authors declare no competing financial interest.

Acknowledgment. This research was supported by Basic Science Research Program through the National Research Foundation of Korea (NRF-2012R1A1A1041869).

Supporting Information Available: The additional figures include the additional SEM, a schematic representation of the power generation mechanism, the NG output performance under reserve-connection mode, a schematic drawing of the bridge rectifier circuit, output performances of the NG under increased stress, etc. The additional movie files (.avi) include the NG output voltages during bending/releasing motions and subsequent lighting up of a red LED. This material is available free of charge via the Internet at <http://pubs.acs.org>.

REFERENCES AND NOTES

- Wang, Z. L.; Song, J. H. Piezoelectric Nanogenerators Based on Zinc Oxide Nanowire Arrays. *Science* **2006**, *312*, 242–246.
- Zhou, J.; Xu, N. S.; Wang, Z. L. Dissolving Behavior and Stability of ZnO Wires in Biofluids: A Study on Biodegradability and Biocompatibility of ZnO Nanostructures. *Adv. Mater.* **2006**, *18*, 2432–2435.
- Omar, K.; Johan Ooi, M. D.; Hassin, M. M. Investigation on Dielectric Constant of Zinc Oxide. *Mod. Appl. Sci.* **2009**, *3*, 110–116.
- Li, P.; Liao, Q.; Yang, S.; Bai, X.; Huang, Y.; Yan, X.; Zhang, Z.; Liu, S.; Lin, P.; Kang, Z.; *et al.* In Situ Transmission Electron Microscopy Investigation on Fatigue Behavior of Single ZnO Wires under High-Cycle Strain. *Nano Lett.* **2014**, *14*, 480–485.
- Arya, S. K.; Saha, S.; Ramirez-Vick, J. E.; Gupta, V.; Bhansali, S.; Singh, S. P. Recent Advances in ZnO Nanostructures and Thin Films for Biosensor Applications: Review. *Anal. Chim. Acta* **2012**, *737*, 1–21.
- Saravanan Kumar, B.; Mohan, R.; Thiagarajan, K.; Kim, S.-J. Fabrication of a ZnO Nanogenerator for Eco-Friendly Biomechanical Energy Harvesting. *RSC Adv.* **2013**, *3*, 16646–16656.
- Chen, C.-Y.; Huang, J.-H.; Song, J.; Zhou, Y.; Lin, L.; Huang, P.-C.; Zhang, Y.; Liu, C.-P.; He, J.-H.; Wang, Z. L. Anisotropic Outputs of a Nanogenerator from Oblique-Aligned ZnO Nanowire Arrays. *ACS Nano* **2011**, *5*, 6707–6713.
- Pradel, Ken C.; Wu, W.; Zhou, Y.; Wen, X.; Ding, Y.; Wang, Z. L. Piezotronic Effect in Solution-Grown P-Type ZnO Nanowires and Films. *Nano Lett.* **2013**, *13*, 2647–2653.
- Gupta, M. K.; Lee, J.-H.; Lee, K. Y.; Kim, S.-W. Two-Dimensional Vanadium-Doped ZnO Nanosheet-Based Flexible Direct Current Nanogenerator. *ACS Nano* **2013**, *7*, 8932–8939.
- Hinchet, R.; Lee, S.; Ardila, G.; Montes, L.; Mouis, M.; Wang, Z. L. Performance Optimization of Vertical

- Nanowire-Based Piezoelectric Nanogenerators. *Adv. Funct. Mater.* **2013**, *24*, 971–977.
11. Yang, Y.; Tian, H.; Sun, H.; Xu, R.-J.; Shu, Y.; Ren, T.-L. A Spring-Connected Nanogenerator Based on ZnO Nanoparticles and a Multiwall Carbon Nanotube. *RSC Adv.* **2014**, *4*, 2115–2118.
 12. Yu, H. K.; Baik, J. M.; Lee, J.-L. Self-Connected and Habitually Tilted Piezoelectric Nanorod Array. *ACS Nano* **2011**, *5*, 8828–8833.
 13. Sohn, J. I.; Cha, S. N.; Song, B. G.; Lee, S. H.; Kim, S. M.; Ku, J. Y.; Kim, H. J.; Park, Y. J.; Choi, B. L.; Wang, Z. L.; et al. Engineering of Efficiency Limiting Free Carriers and an Interfacial Energy Barrier for an Enhancing Piezoelectric Generation. *Energy Environ. Sci.* **2013**, *6*, 97–104.
 14. Hu, Y.; Lin, L.; Zhang, Y.; Wang, Z. L. Replacing a Battery by a Nanogenerator with 20 V Output. *Adv. Mater.* **2011**, *24*, 110–114.
 15. Lee, K. Y.; Kumar, B.; Seo, J.-S.; Kim, K.-H.; Sohn, J. I.; Cha, S. N.; Choi, D.; Wang, Z. L.; Kim, S.-W. P-Type Polymer-Hybridized High-Performance Piezoelectric Nanogenerators. *Nano Lett.* **2012**, *12*, 1959–1964.
 16. Shin, S.-H.; Lee, M. H.; Jung, J.-Y.; Seol, J. H.; Nah, J. Piezoelectric Performance Enhancement of ZnO Flexible Nanogenerator by a CuO–ZnO P–N Junction Formation. *J. Mater. Chem. C* **2013**, *1*, 8103–8107.
 17. Kim, H.; Kim, S. M.; Son, H.; Kim, H.; Park, B.; Ku, J.; Sohn, J. I.; Im, K.; Jang, J. E.; Park, J.-J.; et al. Enhancement of Piezoelectricity via Electrostatic Effects on a Textile Platform. *Energy Environ. Sci.* **2012**, *5*, 8932–8936.
 18. Zhao, M.-H.; Wang, Z.-L.; Mao, S. X. Piezoelectric Characterization of Individual Zinc Oxide Nanobelt Probed by Piezoresponse Force Microscope. *Nano Lett.* **2004**, *4*, 587–590.
 19. Wu, W.; Bai, S.; Yuan, M.; Qin, Y.; Wang, Z. L.; Jing, T. Lead Zirconate Titanate Nanowire Textile Nanogenerator for Wearable Energy-Harvesting and Self-Powered Devices. *ACS Nano* **2012**, *6*, 6231–6235.
 20. Chen, X.; Xu, S.; Yao, N.; Shi, Y. 1.6 V Nanogenerator for Mechanical Energy Harvesting Using PZT Nanofibers. *ACS Nano* **2010**, *10*, 2133–2137.
 21. Wang, Z. L. ZnO Nanowire and Nanobelt Platform for Nanotechnology. *Mater. Sci. Eng., R* **2009**, *64*, 33–71.
 22. Shin, S.-H.; Kim, Y.-H.; Lee, M. H.; Jung, J.-Y.; Nah, J. Hemispherically Aggregated BaTiO₃ Nanoparticle Composite Thin Film for High-Performance Flexible Piezoelectric Nanogenerator. *ACS Nano* **2014**, *8*, 2766–2773.
 23. Wang, X. S.; Wu, Z. C.; Webb, J. F.; Liu, Z. G. Ferroelectric and Dielectric Properties of Li-Doped ZnO Thin Films Prepared by Pulsed Laser Deposition. *Appl. Phys. A: Mater. Sci. Process.* **2003**, *77*, 561–565.
 24. Lin, C.-C.; Chang, C.-C.; Wu, C.-J.; Tseng, Z.-L.; Tang, J.-F.; Chu, S.-Y.; Chen, Y.-C.; Qi, X. In Situ Post-Annealing Technique for Improving Piezoelectricity and Ferroelectricity of Li-doped ZnO Thin Films Prepared by Radio Frequency Magnetron Sputtering System. *Appl. Phys. Lett.* **2013**, *102*, 102107.
 25. Lee, J. S.; Cha, S. N.; Kim, J. M.; Nam, H. W.; Lee, S. H.; Ko, W. B.; Wang, K. L.; Park, J. G.; Hong, J. P. P-Type Conduction Characteristics of Lithium-Doped ZnO Nanowires. *Adv. Mater.* **2011**, *23*, 4183–4187.
 26. Yuan, D.; Guo, R.; Wei, Y.; Wu, W.; Ding, Y.; Wang, Z. L.; Das, S. Heteroepitaxial Patterned Growth of Vertically Aligned and Periodically Distributed ZnO Nanowires on GaN Using Laser Interference Ablation. *Adv. Funct. Mater.* **2010**, *20*, 3484–3489.
 27. Wei, Y.; Wu, W.; Guo, R.; Yuan, D.; Das, S.; Wang, Z. L. Wafer-Scale High-Throughput Ordered Growth of Vertically Aligned ZnO Nanowire Arrays. *Nano Lett.* **2010**, *10*, 3414–3419.
 28. Patra, M. K.; Manzoor, K.; Manoth, M.; Vadera, S. R.; Kumar, N. Studies of Luminescence Properties of ZnO and ZnO:Zn Nanorods Prepared by Solution Growth Technique. *J. Lumin.* **2008**, *128*, 267–272.
 29. Zhang, D. H.; Xue, Z. Y.; Wang, Q. P. The Mechanisms of Blue Emission from ZnO Films Deposited on Glass Substrate by R.F. Magnetron Sputtering. *J. Phys. D: Appl. Phys.* **2002**, *35*, 2837.
 30. Vanheusden, K.; Seager, C. H.; Warren, W. L.; Tallant, D. R.; Voigt, J. A. Correlation between Photoluminescence and Oxygen Vacancies in ZnO Phosphors. *Appl. Phys. Lett.* **1996**, *68*, 403.
 31. Panigrahy, B.; Aslam, M.; Misra, D. S.; Ghosh, M.; Bahadur, D. Defect-Related Emissions and Magnetization Properties of ZnO Nanorods. *Adv. Funct. Mater.* **2010**, *20*, 1161–1165.
 32. Djuricic, A. B.; Leung, Y. H.; Tam, K. H.; Hsu, Y. F.; Ding, L.; Ge, W. K.; Zhong, Y. C.; Wong, K. S.; Chan, W. K.; Tam, H. L.; et al. Defect Emissions in ZnO Nanostructures. *Nanotechnology* **2007**, *18*, 095702.
 33. McCluskey, M. D.; Jokela, S. J. Defects in ZnO. *J. Appl. Phys.* **2009**, *106*, 071101.
 34. Romano, G.; Mantini, G.; Carlo, A. D.; D'Amico, A.; Falconi, C.; Wang, Z. L. Piezoelectric Potential in Vertically Aligned Nanowires for High Output Nanogenerators. *Nanotechnology* **2011**, *22*, 465401.
 35. Yang, R.; Qin, Y.; Dai, L.; Wang, Z. L. Power Generation with Laterally Packaged Piezoelectric Fine Wires. *Nat. Nanotechnol.* **2009**, *4*, 34–39.
 36. Yang, R.; Qin, Y.; Li, C.; Dai, L.; Wang, Z. L. Characteristics of Output Voltage and Current of Integrated Nanogenerators. *Appl. Phys. Lett.* **2009**, *94*, 022905.